Geochemical Perspectives Letters

Mononuclear U(IV) complexes and ningyoite as major uranium species in lake sediments

G. Morin[1]*, A. Mangeret[2], G. Othmane[1], L. Stetten[1,2], M. Seder-Colomina[1,2], J. Brest[1], G. Ona-Nguema[1], S. Bassot[2], C. Courbet[2], J. Guillevic[2], A. Thouvenot[3], O. Mathon[4], O. Proux[5], J.R. Bargar[6]

OPEN ACCESS

Abstract

doi: 10.7185/geochemlet.1610

Natural attenuation of uranium in subsurface environments is usually assigned to immobilisation processes due to microbially mediated reduction of U(VI). Recent laboratory studies have established that the end products of such a process include both low solubility biogenic uraninite and more labile non-crystalline U(IV) species. Indeed, biogenic uraninite formation may be inhibited in the presence of organic or inorganic phosphoryl ligands, leading to the formation of non-crystalline U(IV)-phosphate complexes or nanoscale U(IV)-phosphate solids. Such species have been observed in shallow contaminated alluvial aquifers and can thus be suspected to form in other important environments, among which lacustrine sediments have a global environmental significance since they may represent major uranium accumulation reservoirs in riverine watersheds. Here, on the basis of microscopic, spectroscopic and chemical extraction analyses, we report the occurrence of mononuclear U(IV)-phosphate/silicate complexes, accompanied by nano-crystalline ningyoite-like U(IV)-phosphate minerals, as major scavengers for uranium in lacustrine sediments downstream from a former uranium mine in France. This observation reveals that uranium trapping mechanisms during early diagenesis of lacustrine sediments can virtually exclude uraninite formation, which has important implications for better modelling uranium cycling in natural and contaminated freshwaters. Moreover, our results raise issues concerning the long term fate of mononuclear U(IV) complexes and U(IV) phosphate nano-minerals, especially with respect to re-oxidation events.

1. Institut de Minéralogie, de Physique des Matériaux et de Cosmochimie (IMPMC), UMR 7590 CNRS-UPMC-IRD-MNHN, case 115, 4 place Jussieu, 75252 Paris Cedex 5, France
* Corresponding author (email: guillaume.morin@impmc.upmc.fr)
2. Institut de Radioprotection et de Sûreté Nucléaire, IRSN, PRP-DGE, 31 avenue de la Division Leclerc, 92262 Fontenay-aux-Roses, France
3. Université de Clermont Ferrand, Athos Environment, 63171 Aubière, France
4. European Synchrotron Radiation Facility (ESRF), BP 220, 38043 Grenoble Cedex, France
5. Observatoire des Sciences de l'Univers de Grenoble (OSUG), UMR CNRS 832, Université Grenoble-Alpes, 38041 Grenoble Cedex 9, France - BM30B/CRG-FAME, ESRF, Polygone scientifique Louis Néel, 71 avenue des Martyrs, 38000 Grenoble, France
6. Stanford Synchrotron Radiation Lightsource (SSRL), SLAC National Accelerator National Laboratory, MS 69, 2575 Sand Hill Road, Menlo Park, CA 94025, USA

Received 4 November 2015 | Accepted 25 January 2016 | Published 16 February 2016

Introduction

Redox cycling of uranium exerts a major control on its mobility in the environment because of the low solubility of U(IV) phases compared to that of U(VI) ones (Bargar *et al.*, 2008). In natural anoxic environments such as estuarine and coastal sediments, early diagenesis conditions favour the reduction of U(VI) species into low solubility U(IV) species, which decreases uranium concentrations in overlying waters and sediment pore-waters (Barnes and Cochran, 1993). Researchers addressing remediation of U-contaminated groundwaters have focused on *in situ* biostimulation strategies involving microbial reduction of U(VI) (Wu *et al.*, 2007; Yabusaki *et al.*, 2007) into biogenic uraninite (Suzuki *et al.*, 2005; Bargar *et al.*, 2008) as well as non-uraninite U(IV) phases (Kelly *et al.*, 2008; Bargar *et al.*, 2013; Alessi *et al.*, 2014a; Newsome *et al.*, 2014). *Ex situ* incubations of aquifer sediments under anoxic conditions have highlighted the importance of non-crystalline U(IV) species as major products of microbial reduction of U(VI) (Sharp *et al.*, 2011; Alessi *et al.*, 2014b). In laboratory bioassays, mononuclear U(IV)-phosphate complexes, in which a U(IV) ion coordinates to a PO_4 group, have been especially observed as products of microbial U(VI) reduction (Bernier-Latmani *et al.*, 2010; Fletcher *et al.*, 2010; Sivaswamy *et al.*, 2011). U(IV)-phosphate mineral phases as ningyoite $CaU(PO_4)_2 \bullet 2H_2O$ have also been identified after microbial reduction of dissolved U(VI) in the presence of phosphate (Bernier-Latmani *et al.*, 2010; Lee *et al.*, 2010) or after reduction of U(VI) phosphate mineral phases (Khijniak *et al.*, 2005; Rui *et al.*, 2013). The occurrence and distribution of non-uraninite U(IV) phases in natural systems is however scarcely documented (Qafoku *et al.*, 2009). Recently, Campbell *et al.* (2012) showed that non-crystalline mononuclear U(IV) is present in aquifer sediments at the Rifle site. On the basis of this observation, it can be suspected that non-crystalline U(IV) species may form in other reducing environments, among which lacustrine sediments have a global environmental significance since they represent major uranium accumulation reservoirs in freshwater watersheds. Studies of uranium distribution in lacustrine environments suggested associations of U with organic matter in bottom lake sediments (Ueda *et al.*, 2000; Chappaz *et al.*, 2010) as well as in the water column (Alberic *et al.*, 2000) but no direct determinations of uranium speciation in such environments have been yet reported.

Here we used a combination of X-ray absorption spectroscopy, electron microscopy and selective chemical extraction to investigate uranium speciation in contaminated lake sediments. We show that uranium occurs mainly in the form of mononuclear U(IV)-phosphate/silicate complexes, and to a lesser extent

as nano-crystalline U(IV)-phosphate of the ningyoite-rhabdophane group. This result has major implications for better predicting the behaviour and fate of uranium in lacustrine environments.

Sampling Site and Analytical Methods

Sediment cores were sampled in March 2011 and October 2012, with an Uwitec© gravity corer, in the lake Saint-Clément, in a high U geological background area located ~20 kilometers downstream from the former uranium mine of Bois Noirs/Limouzat in the Massif Central, France (Fig. S-1). Core sections were immediately placed in a glove bag, purged with N_2, sealed in hermetic containers, transported below 4 °C, and dried under vacuum in a glove-box at the IMPMC laboratory 24 hours after sampling. Samples were preserved under anoxic conditions until and during mineralogical and spectroscopic analyses, and during chemical extractions. For SEM-EDXS analyses, sediments were embedded in epoxy resin and prepared as thin sections. Here, we studied the most concentrated samples collected at 120-123 cm and 143-146 cm depth in the 2012 core and at 190-194 cm depth in the 2011 core, with total bulk U contents of ~200, 275 and 360 mg/kg (Fig. S-1; Table S-1). To determine uranium solid-state speciation, we used X-ray Absorption Near Edge Structure (XANES) spectroscopy, Extended X-ray Absorption Fine Structure (EXAFS) spectroscopy at the U L_{III}-edge, and Scanning Electron Microscopy coupled with Energy Dispersive X-ray Spectroscopy (SEM-EDXS) analyses. In addition, we used 1M $NaHCO_3$ O_2-free solution extraction (Alessi *et al.*, 2012) for evaluating the proportion of non-crystalline U(IV) species in the same samples. See Supplementary Information for detailed procedures.

Identification of U-bearing Minerals in the Sediment Samples

X-ray diffraction indicated that the sediments consisted mainly of quartz, feldspar, micas and chlorite, in agreement with their chemical composition (Table S-1) and with the granitic geological substratum (Fig. S-1). The high organic carbon content ~12 wt % was related to fresh organic matter including vegetal debris. Barite [$BaSO_4$] was detected under SEM-EDXS analyses, and pyrite [FeS_2] was present as rare submicron sized crystals. Systematic SEM observations and EDXS analyses of the 143-146 cm sample revealed scarce U-bearing minerals (Table S-2): zircon, thorite (Fig. S-2), monazite (Fig. S-3), rhabdophane (Figs. S-4, S-5), and a nano-crystalline U-rich phosphate mineral of the ningyoite group (Figs. 1, S-6). Ningyoite was the most concentrated U phase identified in the sample, with the following approximate structural formula: $[(U_{0.95}Ca_{0.3}Fe_{0.15}Al_{0.15}Y_{0.4}Nd_{0.05})(PO_4)(SiO_4)\bullet nH_2O]$ (Table S-2, Fig. S-6). According to Muto *et al.* (1959), powder XRD data of ningyoite $[CaU(PO_4)_2\bullet 2H_2O]$ indicate that this mineral is isostructural to rhabdophane $[REE^{3+}PO_4\bullet H_2O]$, with an equivalent amount of U^{4+} and

Ca^{2+} ions substituting for the REE^{3+} ions. In the mineral phase identified here, the excess of U^{4+} over Ca^{2+} is likely compensated by SiO_4^{4-} for PO_4^{3-} substitution, as in Si-rich ningyoite (Doinikova *et al.*, 2014). Most ningyoite ore deposits are suspected to have formed in reducing zones close to the anoxic-oxic boundary, possibly via microbial activity (Doinikova, 2007) as suggested by laboratory experiments (Khijniak *et al.*, 2005; Bernier-Latmani *et al.*, 2010; Lee *et al.*, 2010; Rui *et al.*, 2013). In the sediments studied here, evaluating the importance of the U(IV) mineral phases with respect to other uranium species required both bulk XANES and EXAFS analyses and selective chemical extractions assays.

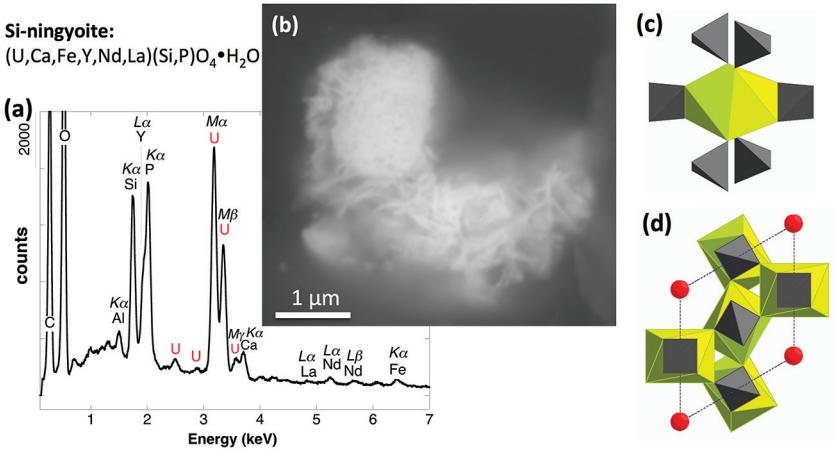

Figure 1 **(a)** EDXS analysis (Table S-2) and **(b)** Backscattered electron SEM image of Si-ningyoite in sample 143-146 cm with nano-sized acicular shaped crystals characteristic of the ningyoite and rhabdophane group minerals. Coordination of the **(c)** $U^{IV}O_8$ polyhedron (yellow) to phosphate tetrahedra (gray), and **(d)** cation polyhedra in the ningyoite/rhabdophane structure (Table S-4).

Uranium Oxidation State

XANES analyses at the U L_{III}-edge indicated that uranium was mainly present as U(IV) in the sediment samples studied (Fig. 2a). Indeed, the shoulder at ~17190 eV that is characteristic of the uranyl ion, *e.g.*, in U(VI)-pyrophosphate (Figs. 3a, S-7), was not observed in the XANES spectra of the sediment samples (Figs. 2a, 7a). Linear Combination Fitting (LCF) of the XANES spectra indicated that the proportion of U(VI) accounted at most for 20 % of total U in the 143-146 cm sample and was below 10 % of total U in the two other sediment samples (Fig. 2a, Table S-3).

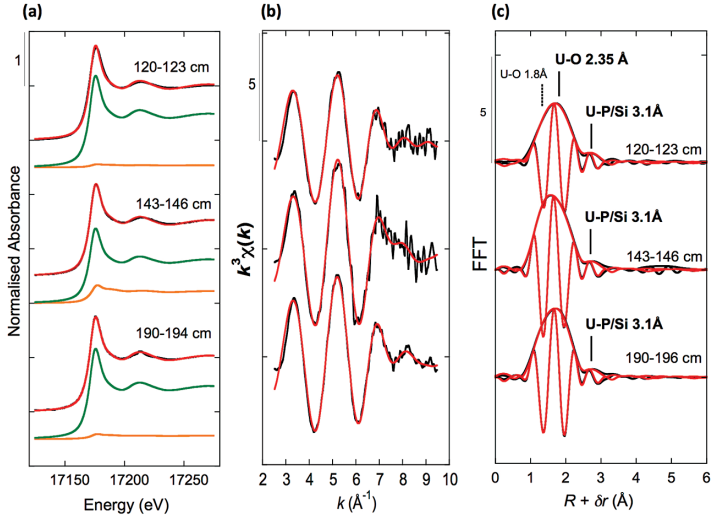

Figure 2 Uranium L_{III}-edge XANES and EXAFS data of the lake sediment samples (black). **(a)** Linear Combination Fits (red) of the XANES spectra included U(IV) citrate (green) and U(VI) pyrophosphate (orange) as components. **(b)** Shell-by-shell fits (red) of the unfiltered $k^3\chi(k)$ EXAFS spectra and **(c)** their Fast Fourier Transforms. See Table S-3 for fitting parameters.

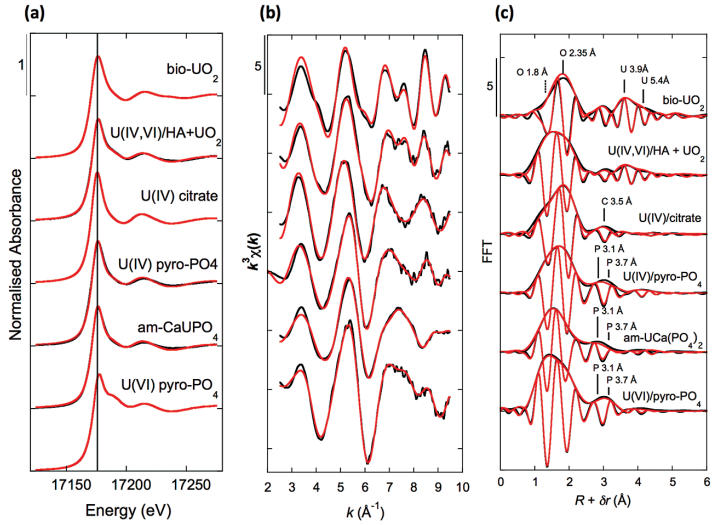

Figure 3 Uranium L_{III}-edge XANES and EXAFS data of relevant model compounds (black). **(a)** Linear Combination Fits (red) of the XANES spectra, **(b)** shell-by-shell fits (red) of the unfiltered $k^3\chi(k)$ functions and **(c)** their Fast Fourier Transforms. See Table S-3 for fitting parameters.

Chemical Extraction as a Probe for Mononuclear U(IV) Species

The proportion of mononuclear U(IV) species in the sediment samples was evaluated by selective chemical extraction using a 1 M $NaHCO_3$ O_2-free solution under anoxic conditions using the protocol of Alessi *et al.* (2012) (Supplementary Information). As shown in Figure 4a, 65 ± 5 % of the total uranium content was extracted from the three samples by this method, and could be assigned to mononuclear U(IV). Indeed, non-crystalline U(IV) species may include mononuclear and polymerised U(IV)-complexes, the latter being less extractable than the former (Alessi *et al.*, 2014b). U(IV)-bearing minerals identified by SEM-EDXS, including ningyoite, rhabdophane, thorite and zircon, thus likely accounted at most for 35 ± 5 % of the total uranium in the sediment samples.

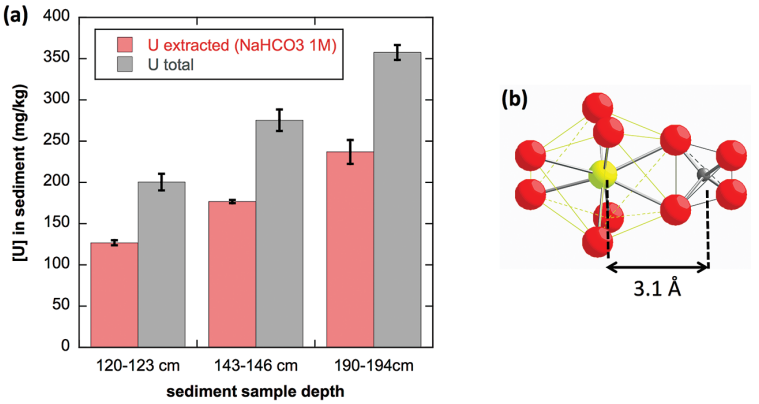

Figure 4 **(a)** Concentration of U(IV) extracted by O_2-free $NaHCO_3$ (1M) solution compared to total bulk U. **(b)** Local structure of mononuclear U(IV)-phosphate/silicate bidendate edge-sharing complexes determined by EXAFS analysis as major solid state species of uranium in the sediments studied (Fig. 2, Table S-3). The phosphate/silicate tetrahedron could be connected to either organic or inorganic substrates.

EXAFS Evidence for Mononuclear U(IV)-phosphate/silicate Complexes as Major U Species

U L_{III}-edge EXAFS data of the three sediment samples were rather similar to each other (Fig. 2b,c), and significantly different from that of biogenic nanouraninite (Fig. 3b,c). Indeed, best fits of the sediment sample data were obtained with 8-9 U-O scattering paths at ~2.35 Å and ~1 U-P or U-Si path at ~3.1 Å, with similar fit quality for a P or Si neighbour (Figs. 2c, S-8, Table S-3). The U-O paths were consistent with U^{4+} ions 8-fold coordinated to oxygen atoms (Table S-4). A minor U-O path at a distance of ~1.8 Å improved the fits, accounting for <5-20 % of uranyl ions identified by XANES analysis (Fig. 2a, Table S-3).

The observed U-P/Si distance of ~3.1 Å corresponds to edge-sharing bidentate bridging of the UO_8 group to a PO_4/SiO_4 tetrahedron (Rui *et al.*, 2013) (Fig. 4b, Table S-4), such U-P distance being characteristic of non-uraninite U(IV) species identified as products of microbial (Bernier-Latmani *et al.*, 2010; Lee *et al.*, 2010; Boyanov *et al.*, 2011) or abiotic (Veeramani *et al.*, 2011) U(VI) reduction. Moreover, a sole P/Si atom was detected beyond the first oxygen coordination sphere of the U absorber, which contrasts with the higher number of second neighbours observed for amorphous U(IV) phases (Table S-3, Fig. S-9). This result demonstrated that uranium was mainly present as mononuclear U(IV)-phosphate/silicate complexes in the sediment, likely accounting for most of the extractable U(IV) fraction (65 ± 5 % of total U in Fig. 4).

Neither the U-U paths of the uraninite structure (Fig. 3), nor the U-P/Si at 3.7-3.8 Å (Fig. 1c) and U-U/Th/Ca/REE paths at 3.6-4.1 Å (Fig. 1d) that are characteristic of crystalline (Table S-4) and amorphous (Fig. S-9) U(IV)–bearing phosphate and silicate mineral phases, were detected around the U absorber in the sediments (Fig. 2c, Table S-3). Owing to the sensitivity of EXAFS to minor components (Alessi *et al.*, 2012), crystalline phases thus accounted for less than 10 % of U, suggesting that the non-extractable U fraction in the sediments (35 ± 5 % of total U in Fig. 4) consisted of nano-crystalline or amorphous U(IV) phases. For instance, biogenic nano-crystalline U(IV) is not easily extracted by 1M $NaHCO_3$ (Alessi *et al.*, 2014b). We thus infer that a fraction of the primary U(IV)-bearing uranium minerals identified by SEM-EDXS, as zircon and thorite are likely metamict because of their high U and Th contents (Table S-2), which would make such phases difficult to detect by EXAFS as minor phases in a mixture with mononuclear U(IV) complexes. Accordingly, ~1 instead of 4 Pu-Zr paths at 3.6 Å were reported for Pu L_{III}-edge EXAFS analysis of highly metamict zircon (Begg *et al.*, 2000). In the same way, ~ 2 to 4 times less P and U neighbours were observed by EXAFS in our amorphous U(IV) model compounds (Table S-3, Fig. 3) than in their crystalline analogues (Table S-4).

Finally, Continuous Cauchy Wavelet Transform analysis of the EXAFS data confirmed that mononuclear U(IV) was mainly complexed to phosphate or silicate groups, even if a minor contribution from carboxylic/phenolic or carbonate groups could not be excluded (Fig. S-8). Hence, our EXAFS results indicated that uranium was mainly in the form of mononuclear U(IV)-phosphate/silicate complexes in the sediments studied and thus provide a direct clue of the importance of such species in lacustrine systems.

Environmental Implications

The knowledge of uranium speciation in natural sediments impacted by anthropogenic activities is essential for predicting the fate of uranium during and after sediment deposition. In that context, lacustrine sediments are of particular importance because they represent important accumulation reservoirs for this element in continental watersheds. The present study yields evidence for

mononuclear U(IV)-phosphate complexes as the main uranium species in lake sediments impacted by a former uranium mine. This observation reveals that uranium trapping mechanisms during early diagenesis of lacustrine sediments can virtually exclude uraninite formation, which has important implications for modelling uranium cycling in natural and contaminated freshwater systems. The absence of uraninite in the sediments studied here supports previous laboratory studies attesting that phosphate ions can inhibit uraninite precipitation (Khijniak *et al.*, 2005; Bernier-Latmani *et al.*, 2010; Lee *et al.*, 2010; Boyanov *et al.*, 2011; Rui *et al.*, 2013), and suggest that silicate could act similarly in natural systems. Our results also indicate that U(IV)-phosphates such as ningyoite, although present, account for a minor fraction of the total U(IV). Such a phase could have formed in the sediment after bioreduction of either soluble U(VI) (Bernier-Latmani *et al.*, 2010) or, more likely, of a secondary U(VI)-phosphate/silicate mineral inherited from the uranium ore (Rui *et al.*, 2013) (Fig. S-1).

Importantly, we show the predominance of mononuclear U(IV)-phosphate/silicate species, in agreement with results of laboratory studies involving U(VI) reduction in the presence of phosphate (Bernier-Latmani *et al.*, 2010; Fletcher *et al.*, 2010; Sivaswamy *et al.*, 2011; Boyanov *et al.*, 2011; Veeramani *et al.*, 2011; Sharp *et al.*, 2011; Alessi *et al.*, 2014b). Such U(IV) mononuclear species could either be sorbed to the surface of phosphate (Veeramani *et al.*, 2011) as well as silicate minerals, or be bound to organic phosphoryl groups (Alessi *et al.*, 2014b). The major occurrence of such species in lacustrine sediments has important environmental implications since mononuclear U(IV) species are potentially more labile than uraninite (Cerrato *et al.*, 2013; Alessi *et al.*, 2014a) and polymerised non-crystalline U(IV) phosphate phases (Alessi *et al.*, 2014b). Such lability raises issues concerning the long term fate of the mononuclear U(IV) species, especially when subjected to sharp redox changes, for example in sediment remediation strategies as dredging operations.

Acknowledgements

We thank Dr. Evelyne Barker, Dr. Imène Esteve and Sebastien Charron, and Loic Martin and Ludovic Delbès, for their help in chemical, SEM, and XRD analyses, respectively. We also thank Prof. Jordi Bruno and another anonymous reviewer for their constructive comments that have helped us to improve the quality of the manuscript. This study was supported by IRSN and CNRS-NEEDS Program. We thank EDF and DREAL Auvergne for having authorised access to the lake of Saint-Clément. The SEM equipment of IMPMC was funded by Région IDF, CNRS, UPMC and ANR. ESRF, French CRG and SSRL facilities are acknowledged for having provided beamtime. SSRL and SLAC are supported by the U.S. Department of Energy (DOE), Office of Science, Office of Basic Energy Sciences under Contract No. DE-AC02-76SF00515, the DOE Office of Biological

and Environmental Research (BER), and by the National Institutes of Health, National Institute of General Medical Sciences (including P41GM103393). Partial support was provided by the U.S. DOE BER and SBR program.

Editor: Rodney C. Ewing

Additional Information

Supplementary Information accompanies this letter at www.geochemicalperspectivesletters.org/article1610

Reprints and permission information is available online at http://www.geochemicalperspectivesletters.org/copyright-and-permissions

Cite this letter as: Morin, G., Mangeret, A., Othmane, G., Stetten, L., Seder-Colomina, M., Brest, J., Ona-Nguema, G., Bassot, S., Courbet, C., Guillevic, J., Thouvenot, A., Mathon, O., Proux, O., Bargar, J.R. (2016) Mononuclear U(IV) complexes and ningyoite as major uranium species in lake sediments. *Geochem. Persp. Let.* 2, 95-105.

References

Alberic, P., Viollier, E., Jezequel, D., Grosbois, C., Michard, G. (2000) Interactions between trace elements and dissolved organic matter in the stagnant anoxic deep layer of a meromictic lake. *Limnology and Oceanography* 45, 1088-1096.

Alessi, D.S., Uster, B., Veeramani, H., Suvorova, E.I., Lezama-Pacheco, J.S., Stubbs, J.E., Bargar, J.R., Bernier-Latmani, R. (2012) Quantitative Separation of Monomeric U(IV) from UO_2 in Products of U(VI) Reduction. *Environmental Science and Technology* 46, 6150-6157.

Alessi, D.S., Lezama-Pacheco, J.S., Janot, N., Suvorova, E.I., Cerrato, J.M., Giammar, D.E., Davis, J.E., Fox, P.M., Williams, K.H., Long, P.E., Handley, K.M., Bernier-Latmani, R., Bargar, J.R. (2014a) Speciation and Reactivity of Uranium Products Formed during in Situ Bioremediation in a Shallow Alluvial Aquifer. *Environmental Science and Technology* 48, 12842-12850.

Alessi, D.S., Lezama-Pacheco, J.S., Stubbs, J.E., Janousch, M., Bargar, J.R., Persson, P., Bernier-Latmani, R. (2014b) The product of microbial uranium reduction includes multiple species with U(IV)-phosphate coordination. *Geochimica et Cosmochimica Acta* 131, 115–127.

Bargar, J.R., Bernier-Latmani, R., Giammar, D.E., Tebo, B.M. (2008) Biogenic uraninite nanoparticles and their importance for uranium remediation. *Elements* 4, 407-412.

Bargar, J.R., Williams, K.H., Campbell, K.M., Long, P.E., Stubbs, J.E., Suvorova, E.I., Lezama-Pacheco, J.S., Alessi, D.S., Stylo, M., Webb, S.M., Davis, J.A., Giammar, D.E., Blue, L.Y., Bernier-Latmani, R. (2013) Uranium redox transition pathways in acetate-amended sediments. *Proceedings of the National Academy of Science of the USA* 110, 4506-4511.

Barnes, C.E., Cochran, J.K. (1993) Uranium geochemistry in estuarine sediments: controls on removal and release processes. *Geochimica et Cosmochimica Acta* 57, 555-589.

Begg, B.D., Hess, N.J., Weber, W.J., Conradson, S.D., Schweiger, M.J., Ewing, R.C. (2000) XAS and XRD study of annealed ^{238}Pu- and ^{239}Pu-substituted zircons ($Zr_{0.92}Pu_{0.08}SiO4$). *Journal of Nuclear Materials* 278, 212-224.

Bernier-Latmani, R., Veeramani, H., Dalla Vecchia, E., Junier, P., Lezama-Pacheco, J.S., Suvorova, E.I., Sharp, J.O., Wigginton, N.S., Bargar, J.R. (2010) Non-uraninite products of microbial U(VI) reduction. *Environmental Science and Technology* 44, 9456-9462.

Boyanov, M.I., Fletcher, K.E., Kwon, M.J., Rui, X., O'Loughlin, E.J., Löffler, F.E., Kemner, K.M. (2011) Solution and microbial controls on the formation of reduced U(IV) phases. *Environmental Science and Technology* 45, 8336-8344.

Campbell, K.M., Kukkadapu, R.K., Qafoku, N.P., Peacock, A.D., Lesher, E., Williams, K.H., Bargar, J.R., Wilkins, M.J., Figueroa, L., Ranville, J., Davis, J.A., Long, P.E. (2012) Geochemical, mineralogical and microbiological characteristics of sediment from a naturally reduced zone in a uranium-contaminated aquifer. *Applied Geochemistry* 27, 1499-1511.

Cerrato, J.M., Asner, M.N., Alessi, D.S., Lezama-Pacheco, J.S., Bernier-Latmani, R., Bargar, J.R., Giammar, D.E. (2013) Relative reactivity of biogenic and chemogenic uraninite and biogenic non crystalline U(IV). *Environmental Science and Technology* 47, 9756-9763.

Chappaz, A., Gobeil, C., Tessier, A. (2010) Controls on uranium distribution in lake sediments. *Geochimica et Cosmochimica Acta* 74, 203-214.

Doinikova, O.A. (2007) Uranium Deposits with a new phosphates types of blacks. *Geology of Ore Deposits* 49, 80-86.

Doinikova, O.A., Sidorenko, G.A., Sivtsov, A.V. (2014) Phosphosilicates of tetravalent uranium. *Doklady Earth Sciences* 456, 755–758.

Fletcher, K.E., Boyanov, M.I., Thomas, S.H., Wu, Q., Kemner, K.M., Löffler, F.E. (2010) U(VI) reduction to mononuclear U(IV) by *Desulfitobacterium* species. *Environmental Science and Technology* 44, 4705-4709.

Kelly, S.D, Kemner, K.M., Carley, J., Criddle, C., Jardine, P.M., Marsh, T.L., Phillips, D., Watson, D., Wu, W.M. (2008) Speciation of uranium in sediments before and after in situ biostimulation. *Environmental Science and Technology* 42, 1558-1564.

Khijniak, T.V., Slobodkin, A.I., Coker, V., Renshaw, J.C., Livens, F.R., Bonch-Osmolovskaya, E.A., Birkeland, N.K., Medvedeva-Lyalikova, N.N., Lloyd, J.R. (2005) Reduction of Uranium(VI) Phosphate during Growth of the Thermophilic Bacterium *Thermoterrabacterium ferrireducens*. *Applied and Environmental Microbiology* 71, 6423-6426.

Lee, S.Y., Baik M.H., Choi, J.W. (2010) Biogenic formation and growth of uraninite (UO_2). *Environmental Science and Technology* 44, 8409-8414.

Muto, T., Meyrowitz, R., Pommer, A., Murano, T. (1959) Ningyoite, a new uranous phosphate mineral from Japan. *American Mineralogist* 44, 633-650.

Newsome, L., Morris, K., Lloyd, J.R. (2014) The biogeochemistry and bioremediation of uranium and other priority radionuclides. *Chemical Geology* 363, 164-184.

Qafoku, N.P., Nikolla, P., Kukkadapu, R.K., Ravi, K., Mckinley, J.P., James, P., Arey, B.W., Kelly, S.D., Wang, C.M., Resch, C.T., Long, P.E. (2009) Uranium in framboidal pyrite from a naturally bioreduced alluvial sediment. *Environmental Science and Technology* 43, 8528-8534.

Rui, X., Kwon, M.J., O'Loughlin, E.J., Dunham-Cheatham, S., Fein, J.B., Bunker, B., Kemner, K. M., Boyanov, M.I. (2013) Bioreduction of Hydrogen Uranyl Phosphate: Mechanisms and U(IV) Products. *Environmental Science and Technology* 47, 5668-5678.

Sharp, J.O., Lezama-Pcheco, J.S., Schofield, E.J., Junier, P., Ulrich, K-U., Chinni, S., Veeramani, H., Margot-Roquier, C., Webb, S.M., Tebo, B.M., Giammar, D.E., Bargar, J.R., Bernier-Latmani, R. (2011) et Uranium speciation and stability after reductive immobilization in aquifer sediments. *Geochimica et Cosmochimica Acta* 75, 6497-6510.

Sivaswamy, V., Boyanov, M.I., Peyton, B.M., Viamajala, S., Gerlach, R., Apel, W.A., Sani, R.K., Dohnalkova, A., Kemner, K.M., Borch, T. (2011) Multiple Mechanisms of Uranium Immobilization by *Cellulomonas sp.* Strain ES6. *Biotechnology and Bioengineering* 108, 264-276.

Suzuki, Y., Kelly, S.D., Kemner, K.A., Banfield, J.F. (2005) Microbial populations stimulated for hexavalent uranium reduction in uranium mine sediment. *Applied Environmental Microbiology* 69, 1337-1346.

Ueda, S., Hasegawa, H., Iyogi, T., Kawabata, H., Kondo, K. (2000) Investigation of physico-chemical form of uranium in sediment of brackish Lake Obushi using sequential extraction procedure. *Limnology* 13, 231-236.

Veeramani, H., Alessi, D., Suvorova, E., Lezama-Pacheco, J., Stubbs, J., Dippon, U., Kappler, A., Bargar, J., Bernier-Latmani, R. (2011) Products of abiotic U(VI) reduction by biogenic magnetite and vivianite. *Geochimica et Cosmochimica Acta* 75, 2512-2528.

Wu, W.M., Carley, J., Luo, J., Ginder-Vogel, M.A., Cardenas, E., Leigh, M.B., Hwang, C.C., Kelly, S.D., Ruan, C.M., Wu, L.Y., Van Nostrand, J., Gentry, T., Lowe, K., Mehlhorn, T., Carroll, S., Luo, W.S., Fields, M.W., Gu, B.H., Watson, D., Kemner, K.M., Marsh, T., Tiedje, J., Zhou, J.Z., Fendorf, S., Kitanidis, P.K., Jardine, P.M., Criddle, C.S. (2007) In situ bioreduction of uranium(VI) to submicromolar levels and reoxidation by dissolved oxygen. *Environmental Science and Technology* 41, 5716-5723.

Yabusaki, S.B., Fang, Y., Long, P.E., Resch, C.T., Peacock, A.D., Komlos, J., Jaffe, P.R., Morrison, S.J., Dayvault, R.D., White, D.C., Anderson, R.T. (2007) Uranium removal from groundwater via in situ biostimulation: field-scale modeling of transport and biological processes. *Journal of Contaminant Hydrology* 93, 216-235.

Mononuclear U(IV) complexes and ningyoite as major uranium species in lake sediments

G. Morin[1]*, A. Mangeret[2], G. Othmane[1], L. Stetten[1,2], M. Seder-Colomina[1,2], J. Brest[1], G. Ona-Nguema[1], S. Bassot[2], C. Courbet[2], J. Guillevic[2], A. Thouvenot[3], O. Mathon[4], O. Proux[5], J.R. Bargar[6]

Supplementary Information

The Supplementary Information includes:

- SI-1: Chemical Analyses Procedures
- SI-2: Selective Chemical Extraction Procedure
- SI-3: Mineralogical Analyses Procedures
- SI-4: Model Compounds Synthesis Procedures
- SI-5: X-Ray Absorption Spectroscopy (XAS) Data Collection
- SI-6: X-Ray Absorption Spectroscopy (XAS) Data Analysis
- SI-7: Tables S-1 to S-4
- SI-8: Figures S-1 to S-9
- Supplementary Information References

1. Institut de Minéralogie, de Physique des Matériaux et de Cosmochimie (IMPMC), UMR 7590 CNRS-UPMC-IRD-MNHN, case 115, 4 place Jussieu, 75252 Paris Cedex 5, France
* Corresponding author (email: guillaume.morin@impmc.upmc.fr)
2. Institut de Radioprotection et de Sûreté Nucléaire, IRSN, PRP-DGE, 31 avenue de la Division Leclerc, 92262 Fontenay-aux-Roses, France
3. Université de Clermont Ferrand, Athos Environment, 63171 Aubière, France
4. European Synchrotron Radiation Facility (ESRF), BP 220, 38043 Grenoble Cedex, France
5. Observatoire des Sciences de l'Univers de Grenoble (OSUG), UMR CNRS 832, Université Grenoble-Alpes, 38041 Grenoble Cedex 9, France - BM30B/CRG-FAME, ESRF, Polygone scientifique Louis Néel, 71 avenue des Martyrs, 38000 Grenoble, France
6. Stanford Synchrotron Radiation Lightsource (SSRL), SLAC National Accelerator National Laboratory, MS 69, 2575 Sand Hill Road, Menlo Park, CA 94025, USA

SI-1: Chemical Analyses Procedures

Sample 2011_190-194cm was analysed for uranium content using the following procedure. Prior to ICP-MS analysis, about 50 mg of powdered sample were dissolved in 2 mL of concentrated HF–HNO_3 mixture, heated at 90 °C for 1h and then evaporated to dryness at 60 °C. The residue was dissolved in 1 mL of HNO_3–H_3BO_3 mixture and slowly evaporated at 60 °C to remove possible weakly soluble fluorides. The new residue was dissolved in 2 % HNO_3 for analysis. Trace element compositions of the digested samples were measured by Inductively Coupled Plasma Mass Spectrometry (ICP-MS) using a X Series II instrument of Thermo Scientific at the University Pierre & Marie Curie.

Samples 2012_120-123 cm and 2012_143-146 cm were analysed for uranium content at the SARM-CRPG laboratory (Nancy, France) by ICP-MS Thermo Elemental X7. The powdered samples were fused with $LiBO_2$ and dissolved with HNO_3 prior to analysis. Major elements were analysed by ICP-OES Thermo Fisher ICap 6500. Details on the analytical procedures can be found at http://www.crpg.cnrs-nancy.fr/SARM/.

SI-2: Selective Chemical Extraction Procedure

Non-crystalline U(IV) species were extracted by reacting 0.1 g of sediment sample with 10 mL of an O_2-free $NaHCO_3$ 1M solution under gentle shaking for 24 hours in an anoxic glove box according to a protocol adapted from Alessi *et al.* (2012). Supernatants were recovered by centrifugation at 6000 rpm for 30 min and filtered through 0.2 µm. An aliquot of 0.5 mL of the supernatant was mixed with 4.5 mL of 1.0 M HNO_3. Dissolved uranium concentrations were then measured by ICP-MS after 100 to 1000 times dilution into 0.1 M HNO_3.

SI-3: Mineralogical Analyses Procedures

Scanning Electron Microscopy analyses were performed using a Zeiss ultra 55 equipped with a Field Emission Gun (FEG) operating at 15 kV with a working distance of 7.5 mm. Images were collected in backscattering mode using the AsB detector. Semi-quantitative analysis of the Energy Dispersive X-ray spectra was performed using the Bruker® Esprit program, by comparison with a standard spectra database and after absorption correction using the Phi(rho,z) method. Calibration of the beam intensity was done using the X-ray emission from a copper grid.

SI-4: Model Compounds Synthesis Procedures

Biogenic uraninite was produced under anoxic conditions at neutral pH by reducing 1.5 mM of uranyl acetate ($UO_2(CH_3COO)_2$•$2H_2O$) in the presence of 20 mM of sodium methanoate as the electron source using a dissimilatory

iron-reducing bacterium *Shewanella oneidensis* MR-1 (5.7 × 108 CFU/mL). The experimental procedures and the composition of the basic medium were similar to those followed by Ona-Nguema *et al.* (2002) and Ona-Nguema *et al.* (2009), with exception of the nature of strain used. The cultures were buffered with 30 mM of $NaHCO_3$ and 20 mM of 1,4-piperazinediethanesulfonic acid (PIPES) as described by Schofield *et al.* (2008). After 24 hours, the solids were harvested by centrifugation at 6000 rpm and vacuum-dried in a dryer placed into a glove-box. The solid was then treated using an O_2-free $NaHCO_3$ 1M solution to remove non-crystalline U species (Alessi *et al.*, 2012) and washed three times with O_2-free deionised water, in order to obtain the solid sample referred to as bio-UO_2.

Acidic U(IV) stock solutions. A 74 mM U(IV) chloride solution was prepared by dissolving 20 mg of bio-UO_2 into 1 mL of 37 % HCl. A 0.2 mM U(IV) chloride solution was prepared by dissolving 5.4 mg of bio-UO_2 into 1 mL of 37 % HCl and completing to 100 mL with O_2-free deionised water.

U(IV,VI) humic acid + UO_2 referred to as "U(IV,VI)/HA + UO_2" was obtained in a Jacomex® anoxic glove box by reacting purified peat humic acid (HA) from Suwanee River obtained from International Humic Substances Society (IHSS) with a 5 10^{-6} M U(IV) solution at acidic pH and rising the pH to 6. For this purpose, 40 mg PPHA was first solubilised in 40 mL O_2-free H_2O at pH 8 under shaking for 24 h. The PPHA solution was then adjusted to pH 3.5 using O_2-free 0.1 M HCl. A volume of 1 mL of a 0.2 mM U(IV) chloride O_2-free solution at pH 1.5 was then added dropwise to the acidified PPHA solution and the pH was then adjusted to 6.5 using a 0.2M NaOH O_2-free solution. The solution was then stirred for 1 h before being evaporated at room temperature under vacuum in the glove box to obtain the sample as a solid paste.

U(IV) citrate was prepared in a Jacomex® anoxic glove box by mixing 1.5 mL of a 260 mM citric acid O_2-free solution at pH 2 (100 mg sodium citrate in 1 mL H_2O + 0.5 mL 35 wt.a % HCl), with 4 mL of a 0.2 mM U(IV) chloride O_2-free solution at pH 1.5, and raising the pH of the mixture to 6.5 with an appropriate volume of 1M NaOH O_2-free solution. The mixed solution was then stirred for 1 h and then evaporated under vacuum within the glove box to obtain U(IV)-citrate as a solid paste.

U(IV) pyrophosphate was prepared in a Jacomex® anoxic glove box by mixing 2.5 mL of a 150 mM pyrophosphoric acid O_2-free solution at pH ~2 (100 mg sodium pyrophosphate in 2 mL deionised O_2-free H_2O + 0.5 mL 85 wt. % H_3PO_4), with 4 mL of a 0.2 mM U(IV) chloride O_2-free solution at pH 1.5, and raising the pH of the mixture to the value of 6.5 with an appropriate volume of 1M NaOH O_2-free solution. The mixed solution was stirred for 1 h and then evaporated under vacuum within the glove box to obtain U(IV)-citrate as a solid paste.

U(VI) pyrophosphate was prepared similarly as the U(IV) pyrophosphate sample but replacing the 4 mL of 0.2 mM U(IV) chloride solution by 0.4 mL of a 2 mM uranyl nitrate solution.

Amorphous CaU(PO$_4$)$_2$•nH$_2$O, was prepared in a Jacomex® anoxic glove box by mixing 20 mL of a 0.74M H_3PO_4 O_2-free solution at pH ~0.8, with 1 mL of a 74 mM U(IV) chloride O_2-free solution at pH -1 and with 0.74 mL of 0.01 M $CaCl_2$ O_2-free solution. The pH was then adjusted to 5 using NaOH O_2-free solution with decreasing molarities and the solution was stirred for 1 hour. The solid was harvested by centrifugation at 6000 rpm for 15 min, washed 3 times with O_2-free deionised H_2O and vacuum-dried in the glove box.

SI-5: X-Ray Absorption Spectroscopy (XAS) Data Collection

Uranium L_{III}-edge XAS data were collected at 15 K on the FAME and BM23 bending magnet beamlines at the European Synchrotron Radiation Facility (ESRF) and on the 11-2 wiggler beamline at the Stanford Synchrotron Radiation Lightsource (SSRL). Data for the 120-123 cm sample and for the am-CaUPO$_4$•nH$_2$O model compound were recorded on the FAME beamline using a 30 elements Ge array fluorescence detector and in transmission mode respectively. Data for the 143-146 cm sample and for all other model compounds were collected on BM23 using a 13 elements Ge array fluorescence detector. U L_{III}-XANES data and U L_{II}-EXAFS data for the 190-194 cm sample were recorded on the 11-2 beamline using a 30 elements Ge array fluorescence detector. The energy of the beam delivered by the Si(111) (BM23) or Si(220) (FAME and 11-2) double-crystal monochromator was calibrated by setting to 17173.4 eV the first inflection point in the U L_{III}-edge of uranyl nitrate recorded in double transmission setup, *i.e.* similar to Zr and Y foils first inflection points calibrated to 17998 and 17038 eV, respectively. A minimum of 12 scans were collected for each sample. Data were averaged, normalised and background subtracted using ATHENA (Ravel and Newville, 2005) to extract experimental XANES and $k^3\chi(k)$ EXAFS functions.

SI-6: X-Ray Absorption Spectroscopy (XAS) Data Analysis

U L_{III}-XANES data of the sediment samples as well as of the model compound samples were fitted using linear combinations (LCF) of the spectra of our purest U(IV) and U(VI) species, namely U(IV) citrate and U(VI) pyrophosphate (Figs. 2a, 3, Table S-3). The quality of the LCF fits was estimated by a *R*-factor: $Rf = \sum [y_{exp} - y_{calc}]^2 / \sum y_{exp}^2$ where y is the normalised absorbance.

U L_{III}-EXAFS data of the sediment samples and of the model compounds were analysed using a classical shell-by-shell fit procedure based on the plane-wave EXAFS formalism (Teo, 1986) and using a Levenberg–Marquardt least-squares minimisation algorithm. Theoretical phase and amplitude functions employed in this fitting procedure were calculated according to the curved-wave scattering theory, thanks to the *ab initio* FEFF8 code (Ankudinov *et al.*, 1998), and using the crystal structures of torbernite (Locock and Burns, 2003) for the U^{VI}–O and U^{VI}–P paths, of $CaU(PO_4)_2$ (Dusausoy *et al.*, 1996) for U^{IV}–O and U^{IV}–P paths, of coffinite (Fuchs and Gebert, 1958) for U^{IV}-Si paths, of uraninite (Wyckoff, 1963)

for U^{IV}–O and U-U paths, and of uranyl acetate dihydrate (Howatson and Grev, 1975) for U–C paths. The quality of this shell-by-shell fit was estimated by using a reduced χ^2 parameter (Table S-3) and by comparing the Continuous Cauchy Wavelet Transform (CCWT) of the experimental and calculated EXAFS spectra (Muñoz *et al.*, 2003, 2005). This latter approach reinforced the identification of the nature of the second-neighbour atoms around uranium.

For the shell-by-shell fitting procedure, the fit quality was estimated using a reduced χ^2 as follows in Equation S-1:

$$\chi^2_R = N_{ind} / [(N_{ind} - N_p)\, n\,] \sum_{i=1,n} [\, k^3\chi(k)exp_i - k^3\chi(k)calc_i\,]^2 / [1+ \varepsilon(k)i^2] \quad \text{Eq. S-1}$$

with $N_{ind} = (2\Delta k \Delta R/\pi)$, the number of independent parameters, N_p the number of free fitting parameters, n the number of fitted data points , $k^3\chi(k)exp_i$ and $k^3\chi(k)calc_i$ the experimental and calculated data point i, and $\varepsilon(k)i$ the measurement uncertainty for each data point i. This latter *v*alue was estimated for each data point i as the Fourier back-transform of the data in the 15-25 Å R-range, following a method modified after Ravel and Newville (2005). Uncertainty on each refined parameter was estimated as , where *VAR(p)* is the variance of parameter p returned by the Levenberg–Marquardt routine for the lowest χ^2_R value.

For the U(VI) pyrophosphate model compound, the number of U-O axial paths found at a distance of 1.77 Å was fixed to $N = 2$ and the number of U-$O_{equatorial}$ paths found at a distance of 2.35 Å was fixed to $N = 5$, in agreement with the geometry of the uranyl ion (Burns, 1999). The 6 multiple scattering paths within the Oax-U-Oax molecule were also added. For the biogenic UO_2 model compound, the number of first oxygen neighbours found at a distance of 2.34 Å was fixed to $N = 8$, as expected from the crystal structure (Wyckoff, 1963).

For all other samples, including model compounds and lake sediment samples, that were dominated by U(IV), the first coordination sphere around U was fitted with a U-O path at a distance of 2.3–2.4 Å with N values varying between 4 and 9, and an additional U-O path at a distance of 1.76–1.79 Å with N values varying between 0 and 1.3. This latter path could be attributed to a minor contribution from uranyl geometry in the lake sediments and in the U(IV) citrate sample and to a more significant one in the U(IV,VI)/HA+UO_2 and U(IV) pyrophosphate samples. In order to better constrain the fitted N value for this path, the corresponding Debye-Waller value was fixed to that obtained after fitting of our pure U(VI) model compound (U(VI) pyrophosphate), *i.e.* 0.05 Å. The expected coordination number for U(IV) is CN = 8 in minerals as UO_2 (Wyckoff, 1963) and can reach CN = 9 in hydrated U(IV) complexes (Hennig *et al.*, 2007), in agreement with the N = 8–9 values of the U-O path at 2.3-2.4 Å found for the lake sediments and our U(IV)-rich model compounds, especially U(IV) citrate. The lower N values found for this U-O path in samples U(IV,VI)/HA+UO_2, U(IV) pyrophosphate and am-CaU(PO$_4$)$_2$•nH$_2$O (N = 4 – 6) is due to the significant proportion of uranyl in these samples (30–50 %).

SI-7: Tables S-1 to S-4

Table S-1 Chemical composition of the samples studied. The uncertainty on last digit is given in parenthesis.

Samples Sampling date	120-123 cm 2012	143-146 cm 2012	190-194 cm 2011
SiO_2 (wt %)	42.5(4)	43.4(4)	n.m.
Al_2O_3 (wt %)	14.6(1)	14.7(1)	14.5(1)
Fe_2O_3 (wt %)	5.2(1)	5.4(1)	6.8(1)
MnO (wt %)	0.08(1)	0.09(1)	0.02(1)
MgO (wt %)	0.95(5)	0.95(5)	1.6(5)
CaO (wt %)	0.64(3)	0.65(3)	0.65(5)
Na_2O (wt %)	0.82(4)	0.85(4)	1.2(1)
K_2O (wt %)	2.3(1)	2.4(2)	1.67(2)
TiO_2 (wt %)	0.73(4)	0.7(4)	0.5(5)
P_2O_5 (wt %)	0.37(4)	0.39(4)	n.m.
T.O.C[#] (wt %)	12.4(5)	12.0(5)	n.m.
L.O.I* (wt %)	31.4	30.0	n.m.
U (ppm)	200(10)	275(14)	358(15)
Th (ppm)	34(2)	36(2)	34(2)
Zr (ppm)	153(12)	167(13)	n.m.
Ba (ppm)	671(33)	784(40)	n.m.
Ce (ppm)	128(6)	134(7)	142(8)
La (ppm)	65(3)	71(4)	78(5)
Nd (ppm)	57(3)	63(3)	70(5)
Y (ppm)	46(2)	51(3)	47(5)

* Loss on ignition; [#] Total Organic Carbon; n.m.: not measured.

Table S-2 SEM-EDXS semi-quantitative analyses of U-bearing mineral phases identified in the 143-146 cm sediment sample. Data are expressed in percentage of oxides with ~15 % relative uncertainties estimated from standard deviations over 2 to 4 analyses. Characteristic molar ratios in mol/mol are given below.

	Si-ningyoite Fig. 1a	rhabdophane Fig. 1b	monazite / rhabdophane Fig. S-4	monazite Fig. S-3	thorite Fig. S-2a	zircon Fig. S-2b
SiO_2	11.0	5.8	0.6	2.5	14.5	23.2
P_2O_5	11.6	19.3	32.7	22.7	9.7	-
UO_2	45.1	3.5	0.5	0.9	5.9	1.5
ThO_2	-	0.6	-	22.4	32.7	0.5
ZrO_2	-	-	-	-	10.5	52.3
HfO_2	-	-	-	-	-	2.2
TiO_2	-	-	-	-	0.4	1.5
La_2O_3	-	5.4	21.7	9.8	-	-
Nd_2O_3	1.0	-	9.4	6.2	-	-
Ce_2O_3	-	15.8	-	35.3	2.3	-
Y_2O_3	7.8	-	-	-	-	-
Al_2O_3	1.5	5.4	0.3	-	5.3	2.7
CaO	2.7	4.3	3.0	0.3	1.7	1.0
FeO	2.5	5.8	-	-	3.6	1.5
MgO	-	0.2	-	-	0.5	0.2
Sum	83.2	66.6	68.2	100.0	87.1	86.8
U/(Si+P)	0.48	0.02	0.004	0.008	0.06	0.015
Th/(Si+P)	-	0.004	-	0.23	0.33	0.005
Zr/(Si+P)	-	-	-	-	0.23	1.10
P/(Si+P)	0.47	0.74	0.98	0.87	0.36	-

Note: symbol (-) indicates values below quantification limit.

Table S-3 Results of XANES Linear Combination fit (LCF) and of EXAFS shell-by-shell fit for the Saint-Clément lake sediment (Fig. 2) and for relevant model compounds (Fig. 3). The XANES LCF components are [a]U(IV) citrate and [b]U(VI) pyrophosphate (Fig S-7). XANES LCF parameters are given in percentage of total uranium in the sample. EXAFS fitting parameters include *R*(Å): interatomic distances; *N*: number of neighbours; σ(Å): Debye Waller factor, ΔE_0(eV): threshold energy shift in electron volts. For each parameter, the uncertainty on last digit is given in parenthesis. *Rf* and χ^2_R are Goodness of Fit parameters. For the sediment samples, the two χ^2_R values refer to fit solutions including P or Si as second neighbour, respectively. Detailed fitting procedure is reported in SI-6.

	XANES				EXAFS					
Sample	**U(IV)[a] ±10 %**	**U(VI)[b] ±10 %**	**Sum (%)**	**Rf (10^{-4})**	**shell**	***R*(Å)**	**N**	**σ (Å)**	**ΔE_0 (eV)**	**χ^2_R**
120-123 cm (2012)	95	<5	99	3.2	U – O U – O U – P/Si	1.76(2) 2.33(2) 3.09(2)	0.3(1) 9(1) 1.0(2)	0.05* 0.13(1) 0.08*	-5(2) - -	2.8/2.9
143-146 cm (2012)	77	21	99	5.7	U – O U – O U – P/Si	1.76(1) 2.33(2) 3.10(2)	0.8(1) 9(1) 1.0(2)	0.05* 0.13(1) 0.08*	-4(2) - -	3.7/3.9
190-194 cm (2011)	94	6	99	8.2	U – O U – O U – P/Si	1.76(1) 2.34(1) 3.09(2)	0.6(1) 9(1) 0.9(2)	0.05* 0.13(1) 0.08*	-4(1) - -	1.6/1.7
UO_2-bio	100*				U – O U – U U – O U – U	2.34(1) 3.85(1) 4.51(3) 5.38(5)	8* 8(5) 13(13) 2(2)	0.12(1) 0.09(2) - -	-2(1) - - -	8.9
U(IV,VI)/ HA + UO_2	49	50	99	0.7	U – O U – O U – C U – U U – O U – U	1.79(1) 2.35(1) 3.38(3) 3.87* 4.53* 5.47*	1.3(1) 5(1) 3(1) 5(1) 9(1) 2(1)	0.05* 0.09(1) - - - -	1(1) - - - - -	6.0
U(IV) citrate	100*				U – O U – O U – C	1.79(1) 2.39(1) 3.50(2)	0.6(1) 9(1) 6(2)	0.05* 0.11(1) -	-1(1) - -	4.4
U(IV) pyro-phosphate	68	31	99	1.5	U – Oax U – O U – P U – P U – U	1.78(1) 2.34(1) 3.12(2) 3.70(2) 4.14(2)	0.9(1) 5.4(8) 1.4(5) 2.2(9) 1.2(7)	0.05* 0.08(1) 0.07(3) - -	-1(1) - - - -	3.0
am-CaU $(PO_4)_2$• nH_2O	58	40	98	2.0	U – Oax U – O U – P U – P U – U	1.77(1) 2.30(2) 3.13(3) 3.69(5) 4.43(4)	1.1(1) 5.9(9) 1.3(7) 0.8(3) 0.6(4)	0.05* 0.11(1) 0.06(6) - -	-2(3) - - - -	2.1
U(VI) pyro-phosphate		100*			U – Oax MS U – Oeq U – P U – P U – U	1.77(1) 3.54* 2.35(1) 3.10(2) 3.64(2) 4.13(3)	2* 6* 5* 1.2(2) 1.6(4) 0.6(3)	0.05(1) - 0.07(1) - - -	-2(1) - - - - -	3.0

Note: (-) linked to the parameter above in the table; (*) fixed parameter.

Table S-4 Selected bond distances calculated from available crystal structure data for U(IV)-bearing phosphate and silicate minerals relevant to the present study. The U^{4+} ion is 8-fold coordinated to oxygen atoms at an average distance of <2.37 Å> in synthetic $CaU(PO_4)_2$, a xenotime-analogue of ningyoite, as well as in coffinite and uraninite (Wyckoff, 1963). The U-P distances at ~3.1 Å and at ~3.7 Å correspond to edge-sharing bidentate bridging, and corner-sharing monodentate bridging, respectively, of the UO_8 group to a PO_4 tetrahedron. Both U-P distances are expected in ningyoite that has a rhabdophane structure (Muto *et al.*, 1959) (Fig. 1c). This UO_8-PO_4 bridging scheme is similar to the UO_8-SiO_4 bridging scheme in coffinite group minerals. In addition, in these various mineral structures, the MeO_8 polyhedron shares edges with MeO_8 polyedra within the 3.6-4.1 Å distance range (Fig. 1d). None of these U-Me paths is observed in the EXAFS data of our sediment samples (Fig. 2, Table S-3).

Mineral species	**paths**	***R*(Å)**	**paths**	***R*(Å)**	**paths**	***R*(Å)**	**References**
ningyoite, $CaU(PO_4)_2$•$2H_2O$	8 U-O	n.a.	2 U-P 2 U-P	n.a. n.a.	4 U-Ca	n.a.	Muto *et al.* (1959)
rhabdophane(Ce), $CePO_4$•$2H_2O$	8 Ce-O	< 2.49 >	2 Ce-P 4 Ce-P	3.22 3.65	4 Ce-Ce	4.13	Mooney (1948)
synthetic $CaU(PO_4)_2$ (isotructural to xenotime $REEPO_4$	8 U-O	< 2.37 >	2 U-P 4 U-P	< 3.07 > < 3.71 >	3 U-Ca 2 U-Ca	< 3.84 > < 4.60 >	Dusausoy *et al.* (1996)
coffinite, $USiO_4$	8 U-O	< 2.37 >	2 U-Si 4 U-Si	3.13 3.83	4 U-U	3.83	Labs *et al.* (2014)
thorite, $ThSiO_4$	8 Th-O	< 2.42 >	2 Th-Si 4 Th-Si	3.15 3.92	4 Th-Th	3.92	Labs *et al.* (2014)
zircon, $ZrSiO_4$	8 Zr-O	< 2.20 >	2 Zr-Si 4 Zr-Si	2.99 3.62	4 Zr-Zr	3.62	Hazen and Finger (1979)

Note: n.a.: crystal structure not available; < > indicates average distance over a given coordination shell.

SI-8: Figures S-1 to S-9

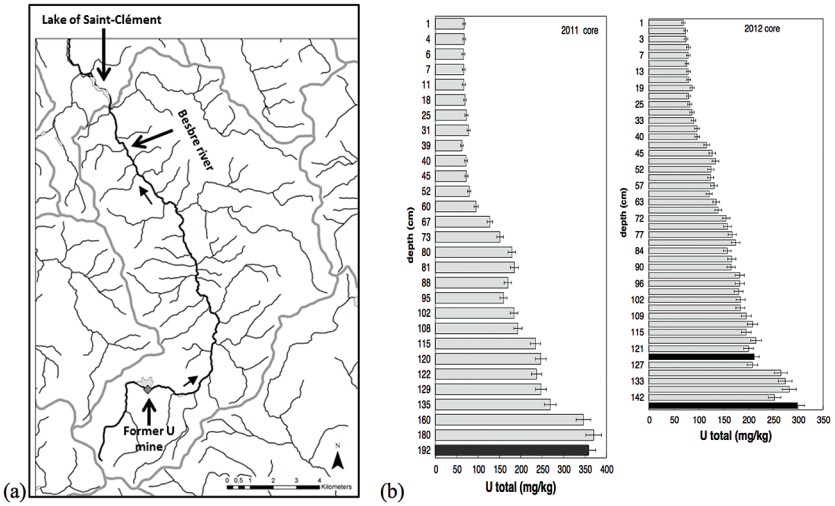

Figure S-1 (a) Sampling site location and **(b)** uranium content in the sediments studied. Bottom lake sediments were cored in Lake Saint-Clément located in Allier, Massif Central, France. The lake is supplied by the Besbre River that drains the discharges from the Bois-Noirs treated mine water, located 20 km upstream from the lake. The uranium ore body of Bois Noirs is a hydrothermal vein deposit hosted by a Hercynian granite. The major mineralisation consists of pitchblende/uraninite [UO_{2+x}] partly replaced by coffinite [$USiO_4$], deposited with minor pyrite and marcasite [FeS_2] in massive quartz [SiO_2] veins (Cuney, 1978). Supergene weathering formed secondary uranyl minerals, mostly torbernite [$Cu(UO_2)_2(PO_4)_2$•8-12(H_2O)], uranophane [$Ca(UO_2)_2SiO_3(OH)_2$•5(H_2O)] and uranopilite [$(UO_2)_6(SO_4)O_2(OH)_6(H_2O)_6$]•8($H_2O$)]. Granitic accessory minerals as zircon [$ZrSiO_4$], thorite [$ThSiO_4$] and monazite [$REEPO_4$] are considered as the primary uranium source for the hydrothermal deposit. About 7000 t of U were extracted between 1958 and 1980 and about 1.3 Mt of fine mill tailings are stored in a pond closed by a dam, from which percolating waters are treated (IRSN, 2015). The U content in the bottom lake sediments of Lake Saint-Clément increases regularly with depth down to about 1.5 to 2 meters depth. In order to facilitate the determination of uranium speciation in the present study, we focused on three concentrated deep sediment samples indicated in black colour in **(b)**. Chemical analysis procedures are reported in Supplementary Information S-1 and complete analysis of the three samples studied is reported in Table S-1.

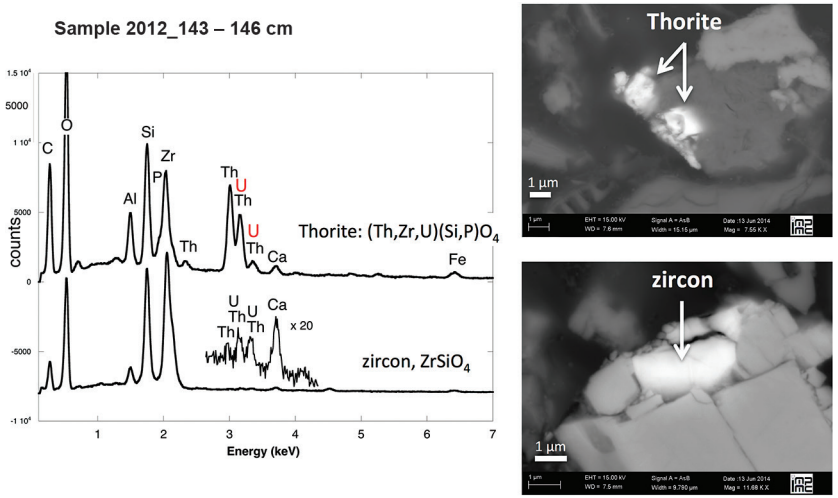

Figure S-2 Backscattered electrons SEM image and SEM-EDXS analyses of uranium–rich P-thorite (auerlite) and zircon crystals in the sediment sample 2012_143-146cm. Corresponding semi-quantitative analyses are reported in Table S-1.

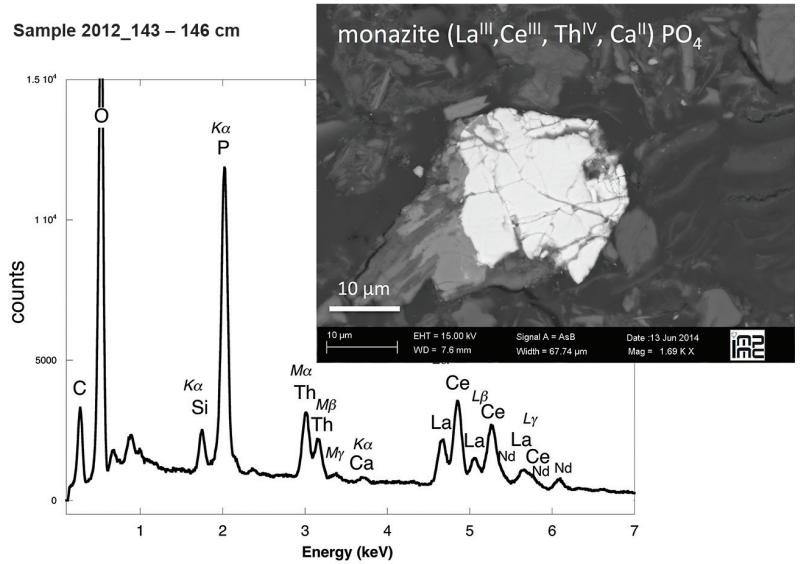

Figure S-3 Backscattered electrons SEM image and SEM-EDXS analysis of Th-monazite in the 2012_143-146cm sediment samples. Corresponding semi-quantitative analyses are reported in Table S-2.

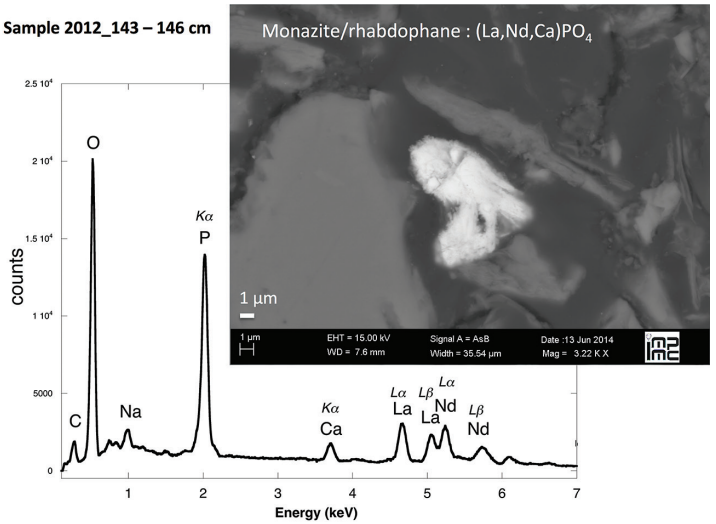

Figure S-4 Backscattered electrons SEM image and SEM-EDXS analysis of monazite grain coated by aggregates of rhabdophane crystals with characteristic acicular shape, in the 2012_143-146 cm sediment sample. Corresponding semi-quantitative analysis are reported in Table S-2.

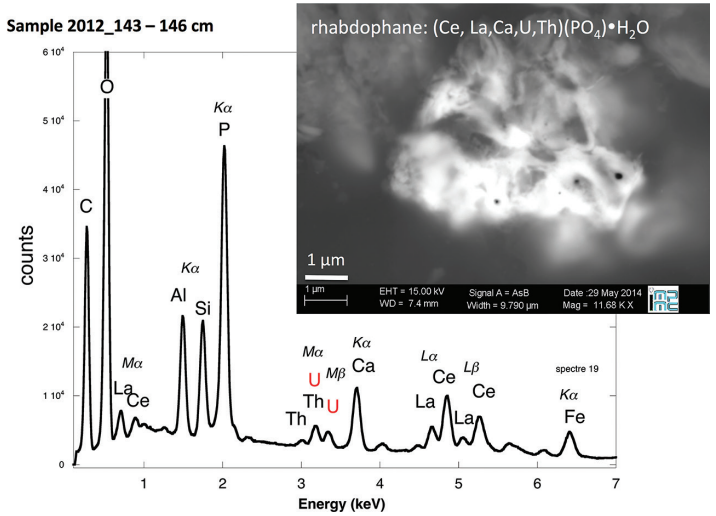

Figure S-5 Backscattered electrons SEM image and SEM-EDXS analysis of U-rich rhabdophane aggregate, in the 2012_143-146 cm sediment sample. Corresponding semi-quantitative analysis are reported in Table S-2.

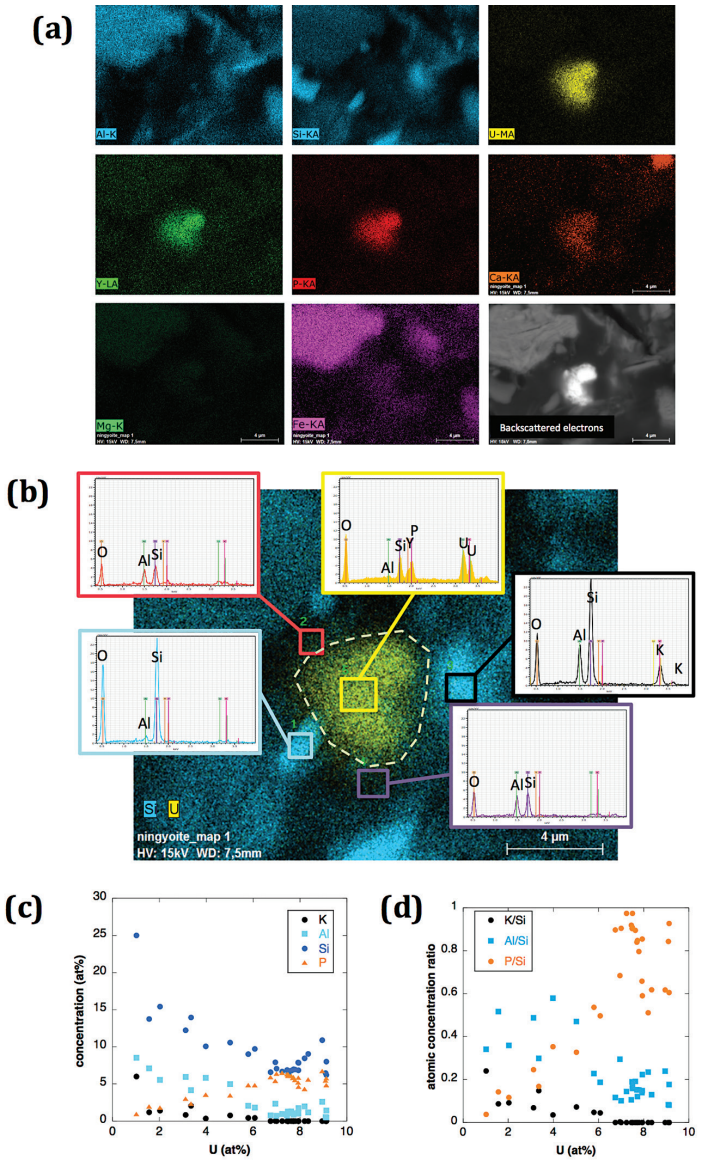

Figure S-6 **(a)** Additional SEM-EDXS data for the area surrounding the Si-ningyoite grain shown in Figure 1, including: elemental maps obtained from integrated intensity of specific emission lines. **(b)** Spectra of specific areas in and around the Si-ningyoite grain. **(c)** Elemental compositions obtained from 25 punctual analyses within the dashed area given in atomic concentrations. **(d)** Atomic concentration ratios. These data indicate that the composition of

the Si-ningyoite grain can be isolated from that of surrounding K-feldspar, quartz and clays particles, which exhibit different Al/Si, and K/Si ratios. This result is consistent with the classical ~1 μm^3 interaction volume of a SEM probe, especially in a heavy material as a U-phosphate mineral. Semi-quantitative analysis obtained from four EDX spectra with high counting rate (0.5 – 1 million counts) is given in Table S-2.

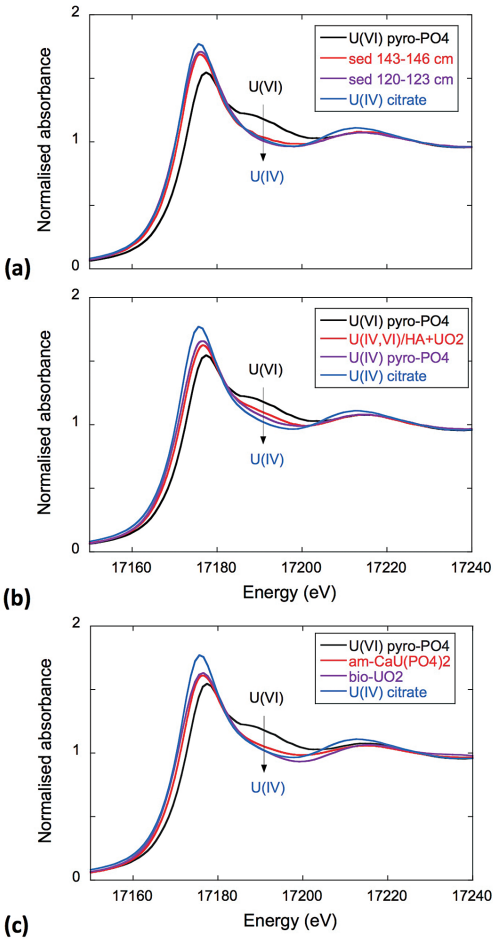

Figure S-7 U L_{III}-edge XANES spectra for the U(IV) and U(VI) model compounds, namely U(IV) citrate and U(VI) pyrophosphate, compared to **(a)** two of the studied sediment samples, **(b)** the U(IV) pyrophosphate and the U(IV,VI)/HA+UO_2 model compounds, and **(c)** the biogenic UO_2 and the amorphous $CaU(PO_4)_2$•nH_2O model compounds. Among our model compounds spectra, U(IV)-citrate and U(VI)-pyrophosphate were chosen as fitting components since they exhibited the purest U(IV) and U(VI) compositions, as compared to our other model compounds (Table S-3).

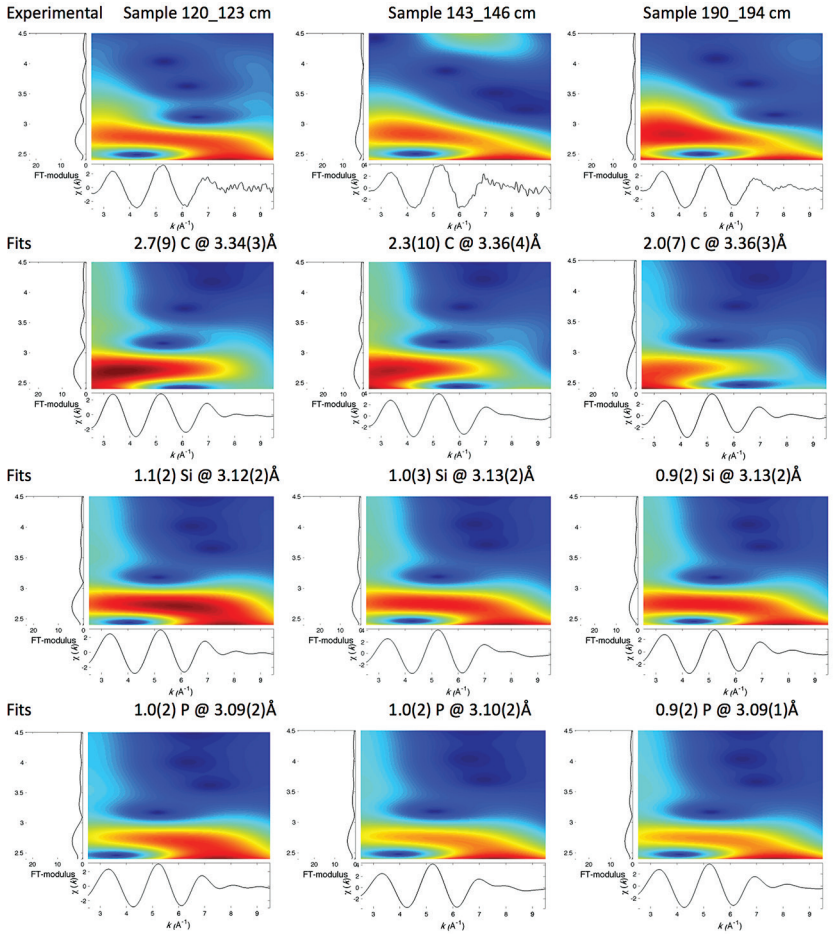

Figure S-8 Continuous Cauchy-Wavelet transform (CCWT) of U L_{III}-edge EXAFS data for the three lake sediment samples studied (from left to right) compared to CCWT of shell-by-shell fits with C, Si or P atoms as second neighbours (from top to bottom). The fits with ~2.5 U-C paths reasonably matched the experimental k^3-EXAFS and FT but yielded χ^2_R ~20 % larger than the U-P or U-Si fits reported in Table S-3 and Figure 3. Moreover, the strong CCWT signal at k < 5 Å^{-1} arising from the C atoms poorly matched the CCWT of the experimental data compared to the CCWT of the P or Si fits. However, potential bonding of U(IV) to carboxylic/phenolic or carbonate groups, in addition to phosphate/silicate groups, cannot be excluded, since CCWT of the experimental data suggests a minor contribution of C atoms at k < 5 Å^{-1}, especially for sample 190-194 cm. Uncertainties on the fit parameters are given in parentheses and refer to the last digit (Table S-3, Fig. 3). The colour code corresponds to the EXAFS signal intensity in arbitrary units, increasing from blue to red. The ordinate axis corresponds to the distance $R+\Delta r$ (Å) from the U absorbing atom, uncorrected from phase-shift. The CCWT analysis was limited to the 2.4-4.5 Å $R+\Delta r$-range, in order to avoid the high intensity EXAFS signal from the first neighbour oxygen atoms around the U absorbing atom.

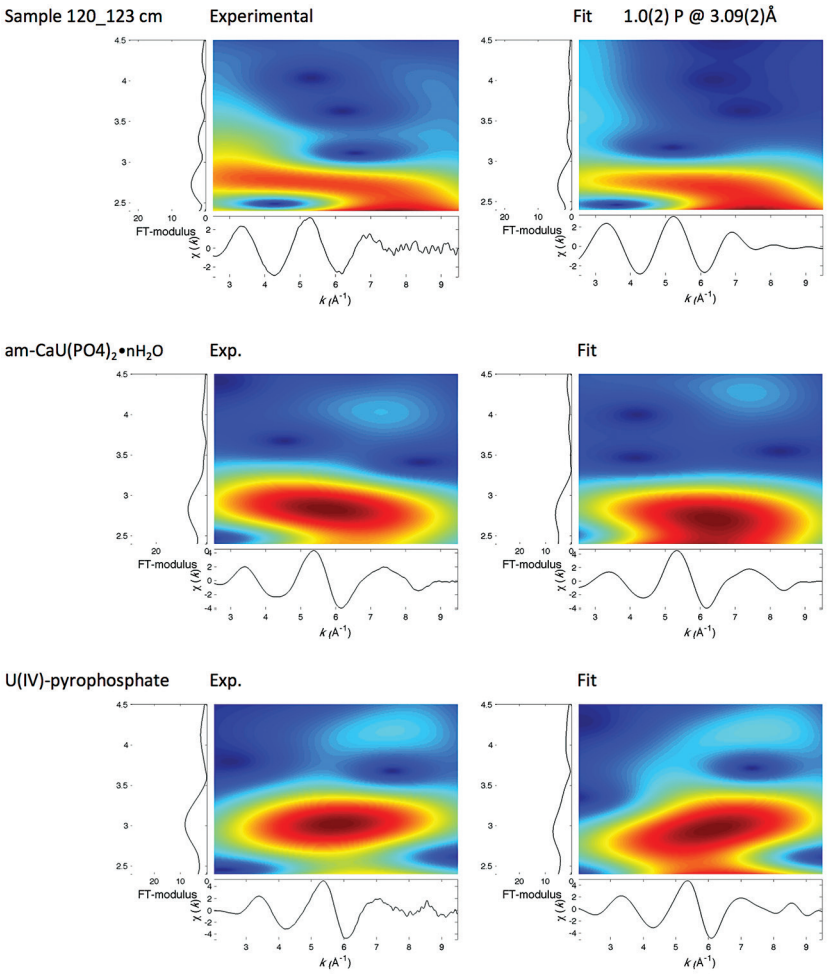

Figure S-9 Continuous Cauchy-Wavelet transform (CCWT) of U L_{III}-edge EXAFS data for the 120-123 cm depth lake sediment samples compared to the data for amorphous U(IV)-phosphate inorganic model compounds. CCWT of both data (left) and fits (right) show that, compared to a single P/Si second neighbour atom observed at R ~3.1 Å in the sediment samples, the contributions from U-P paths at R ~3.1 and 3.7 Å, centred at k ~5.5 $Å^{-1}$ is sharp for the amorphous model compounds, as also indicated by the fitting results (Table S-3, Fig. 3). An additional U-U path at R ~4.1-4.3 Å, centered at k ~8 $Å^{-1}$, is observed for U(IV)-pyrophosphate, and, to a lesser extent, for am-$CaU(PO_4)_2•nH_2O$, whereas this contribution is absent for the sediment samples. Corresponding fitting parameters are reported in Table S-3. The CCWT analysis was limited to the 2.4-4.5 Å $R+\Delta r$-range, uncorrected for phase shift, in order to avoid the high intensity EXAFS signal from the first neighbour oxygen atoms around the U absorbing atom.

Supplementary Information References

Alessi, D.S., Uster, B., Veeramani, H., Suvorova, E.I., Lezama-Pacheco, J.S., Stubbs, J.E., Bargar, J.R., Bernier-Latmani, R. (2012) Quantitative Separation of Monomeric U(IV) from UO_2 in Products of U(VI) Reduction. *Environmental Science and Technology* 46, 6150-6157.

Ankudinov, A.L., Ravel, B., Rehr, J.J., Conradson, S.D. (1998) Real-space multiple-scattering calculation and interpretation of x-ray-absorption near-edge structure. *Physical Review B* 58, 7565–7576.

Burns, P.C. (1999) The crystal chemistry of uranium. In: Burns, P.C., Finch, R. (Eds.) *Uranium: Mineralogy, Geochemistry and the Environment.* Mineralogical Society of America, Washington DC, 23–90.

Cuney, M., (1978) Geologic Environment, Mineralogy, and Fluid Inclusions of the Bois Noirs-Limouzat Uranium Vein, Forez, France. *Economic Geology* 73, 1567-1610.

Dusausoy, Y., Ghermani, N.E., Podor, R., Cuney, M. (1996) Low-temperature ordered phase of $CaU(PO_4)_2$: synthesis and crystal structure. *European Journal of Mineralogy* 8, 667-673.

Fuchs, L.H., Gebert, E. (1958) X-ray studies of synthetic coffinite, thorite and uranothorites. *American Mineralogist* 43, 243-248.

Hazen, R.M., Finger, L.W. (1979) Crystal structure and compressibility of zircon at high pressure. *American Mineralogist* 64, 196-201.

Hennig, C., Schmeide, K., Brendler, V., Moll, H., Tsushima, S., Scheinost, A.C. (2007) EXAFS Investigation of U(VI), U(IV), and Th(IV) Sulfato complexes in aqueous solution. *Inorganic Chemistry* 46, 5882–5892.

Howatson, J., Grev, D.M. (1975) Crystal and molecular structure of uranyl acetate dihydrate. *Journal of Inorganic and Nuclear Chemistry* 37, 1933–1935.

IRSN (2015) http://mimausabdd.irsn.fr/index.php/Report/synthesisReport?code_site=42SU03

Labs, S, Hennig, C., Weiss, S., Curtius, H., Zan̈ker, H., Bosbach, D. (2014) Synthesis of Coffinite, $USiO_4$, and structural investigations of $UxTh(1–x)SiO_4$ Solid Solution. *Environmental Science and Technology* 48, 854–860.

Locock, A.J., Burns, P.C. (2003) Crystal structures and synthesis of the copper-dominant members of the autunite and meta-autunite groups: torbernite, zeunerite, metatorbernite and metazeunerite. *Canadian Mineralogist* 41, 489-502.

Mooney, R.C.L. (1948) Crystal structures of a series of rare earth phosphates. *Journal of Chemical Physics* 16, 1003-1003.

Muñoz, M., Argoul, P., Farges, F. (2003) Continuous Cauchy wavelet transform analyses of EXAFS spectra : A qualitative approach. *American Mineralogist* 88, 694–700.

Muñoz, M., Farges, F., Argoul, P. (2005) Continuous Cauchy Wavelet Transform of XAFS Spectra. *Physica Scripta* 221–222.

Muto, T., Meyrowitz, R., Pommer, A., Murano, T. (1959) Ningyoite, a new uranous phosphate mineral from Japan. *American Mineralogist* 44, 633-650.

Ona-Nguema, G., Abdelmoula, M., Jorand, F., Benali, O., Géhin, A., Block, J.-C., Génin, J.-M.R. (2002) Iron(II,III) hydroxycarbonate green rust formation and stabilisation from lepidocrocite bioreduction. *Environmental Science and Technology* 36, 16-20.

Ona-Nguema, G., Morin, G., Wang, Y., Menguy, N., Juillot, F., Olivi, L., Aquilanti, G., Abdelmoula, M., Ruby, C., Bargar, J.R., Guyot, F., Calas, G., Brown, J.R.G.E. (2009) Arsenite sequestration at the surface of nano-$Fe(OH)_2$, ferrous-carbonate hydroxide, and green-rust after bioreduction of arsenic-sorbed lepidocrocite by Shewanella putrefaciens. *Geochimica et Cosmochimica Acta* 73, 1359-1381.

Ravel, B., Newville, M. (2005) ATHENA, ARTEMIS, HEPHAESTUS: data analysis for X-ray absorption spectroscopy using IFEFFIT. *Journal of Synchrotron Radiation* 12, 537–541.

SCHOFIELD, E.J., VEERAMANI, H., SHARP, J.O., SUVOROVA, E., BERNIER-LATMANI, R., MEHTA, A., STAHLMAN, J., WEBB, S.M., CLARK, D.L., CONRADSON, S.D. (2008) Structure of biogenic uraninite produced by Shewanella oneidensis strain MR-1. *Environmental Science and Technology* 42, 7898-7904.

TEO, B.K. (1986) EXAFS: Basic principles and data analysis. Springer Berlin Heidelberg, Berlin.

WYCKOFF, R.W.G. (1963) Crystal Structures 1. Second Edition, Interscience Publishers, New York, 239–444.